

This is the **accepted version** of the journal article:

Romero Fernández, Nuria; Barrach Guerra, Renan; Gil Jiménez, Laia; [et al.].
«TiO₂-mediated visible-light-driven hydrogen evolution by ligand-capped Ru
nanoparticles». Sustainable Energy and Fuels, Vol. 4, Issue 8 (August 2020), p.
4170-4178. DOI 10.1039/d0se00446d

This version is available at <https://ddd.uab.cat/record/273904>

under the terms of the  ^{IN} COPYRIGHT license

ARTICLE

TiO₂-Mediated Visible-Light-Driven Hydrogen Evolution by Ligand-Capped Ru Nanoparticles

Received 00th January 20xx,
Accepted 00th January 20xx

Nuria Romero,^[a] Renan Barrach Guerra,^[b] Laia Gil,^[a] Samuel Drouet,^[c] Ivan Salmeron-Sánchez,^[a] Ona Illa,^[a] Karine Philippot,^[c] Mirco Natali,^{[d]*} Jordi García-Antón,^{[a]*} Xavier Sala.^{[a]*}

DOI: 10.1039/x0xx00000x

Ru nanomaterials have recently emerged as potential substitutes for classical Pt-based cathodes in the hydrogen evolution reaction (HER). In this regard, nanoparticle surface-functionalization through the so-called organometallic approach is a promising strategy towards the synthesis of tailored highly active and durable HER (photo)electrocatalyst of limitless tunability. Herein, efficient (turnover numbers over 480 mol_{H₂} · mol_{Ru}⁻¹ and turnover frequencies of 21.5 mol_{H₂} · h⁻¹ · mol_{Ru}⁻¹, apparent quantum yield of 1.3%) and durable (> 100 h) visible-light-driven hydrogen evolution has been achieved at neutral pH with a ternary hybrid nanomaterial combining 4-phenylpyridine-capped Ru nanoparticles (RuPP), TiO₂ nanocrystals and [Ru(bpy)₂(4,4'-(PO₃H₂)₂(bpy))]Cl₂ (RuP) using triethanolamine (TEOA) as sacrificial electron-donor. Photophysical analysis by means of transient absorption spectroscopy has been performed in order to shed light on the kinetics of the electron transfer events and to identify the rate-determining step of the overall photocatalytic process. TiO₂ is shown to have a key role as (1) support aiding the dispersion of the photocatalyst and limiting its agglomeration under turnover conditions and, (2) electron-transfer mediator enabling the efficient electron-communication between the catalyst and the anchored molecular photoabsorber. Finally, the evolution and fate of the photocatalyst on long-term HER photocatalysis are thoroughly analyzed.

Introduction

The effects of global warming, triggered by the massive combustion of fossil resources, threaten our societal lifestyle and urge the development of sustainable energy conversion schemes. Inspired by the light-driven production of biomolecules in photosynthetic processes, storing sunlight energy in the chemical bonds of a fuel is a promising strategy known as artificial photosynthesis.^[1] In this regard, the sustainable production of molecular hydrogen through sunlight-driven water splitting (*hν*-WS) is a key process as the obtained H₂ can be directly used as a fuel or employed as a reagent for other relevant routes such as the production of green methanol through CO₂-based processes.^[2]

In a *division-of-labor* approach for *hν*-WS, photoelectrochemical (PEC) cells represent a compromise between technological maturity and cost, relying on the development of individual photoanodes and photocathodes.^[3,4] In *hν*-WS PEC cells, solar energy is collected by light-harvesting components that enable light-induced charge separation after excitation, water serves as an electron and proton

donor at the photoanode and protons are converted into dihydrogen at the photocathode. Thus, the development of efficient photocatalytic systems for the hydrogen evolution reaction (HER) is a central matter in *hν*-WS. In this endeavor, appropriate HER photocatalysts and photoabsorber (PA) molecules/materials must be developed and properly combined in order to minimize undesired charge recombination processes.

Even if relatively low-demanding from a thermodynamic point of view (E⁰(H₂O/H₂) = -0.41 V vs. NHE at pH 7), the two-electron reduction of protons to molecular hydrogen is kinetically sluggish and requires the use of appropriate catalysts. Pt, with low working overpotentials and extremely high intrinsic activities (due to the ideal Pt-H adsorption energy), is regularly the metal of choice.^[5] Nevertheless, heterogeneous Pt-based systems suffer from (a) important corrosion under alkaline conditions, and (b) the scarcity and prohibitive price of the metal that makes it unsuitable for practical large-scale applications. In view of the limited HER performance of most earth-abundant systems,^[6] Ru nanomaterials have recently emerged as potential substitutes to Pt-based cathodes.^[7–9] Ru-based systems are an alternative to reduce the cost of the catalyst (since the price of Ru is ¼th that of Pt) but mainly to overcome the stability issues in alkaline conditions of the latter. In this regard, we have recently highlighted the power of the organometallic approach^[10] for the tailored development of ligand-capped Ru nanoparticles (NPs) that display narrow size-distribution and controllable surface properties, as well as high electrocatalytic performance and long-term durability for HER.^[11,12] Despite their relevant electrocatalytic performance, the number of efficient HER photocatalytic systems based on Ru nanocatalysts is still very limited.^[9] Together with their frequent agglomeration under

^a Departament de Química, Universitat Autònoma de Barcelona, 08193-Bellaterra, Barcelona, Spain. E-mail: Jordi.GarciaAnton@uab.es; Xavier.Sala@uab.cat

^b UNICAMP - Instituto de Química, I-102, Postal box 6154 CEP 13083-970 Cidade Universitária - Campinas, SP, Brasil.

^c Dr. Samuel Drouet, Dr. Karine Philippot, LCC-CNRS, Université de Toulouse, CNRS, UPS, 205, route de Narbonne, F-31077 Toulouse, France.

^d Dipartimento di Scienze Chimiche e Farmaceutiche, Università degli Studi di Ferrara and Centro Interuniversitario SolarChem, sez. di Ferrara, Via L. Borsari, 46, 44121 Ferrara, Italy. E-mail: mirco.natali@unife.it

† Electronic Supplementary Information (ESI) available: See DOI: 10.1039/x0xx00000x

turnover conditions,^[13] the attainment of a charge-separated state in PA (i.e. $[\text{Ru}(\text{bpy})_3]^{2+}$ derivatives, see Chart 1) / Ru NP systems is typically hampered by non-desired back-electron transfer processes from the PA excited state.^[14] Thus, together with a sacrificial electron-donor, the use of an electron relay (i.e. methyl viologen) is often required. Relevant exceptions were reported by Fukuzumi and co-workers using organic donor-acceptor linked dyads (i.e. the 2-phenyl-4-(1-naphthyl)-quinolinium ion, $\text{QuPh}^+\text{-NA}$, see Chart 1) which afford long-lived charge-separated states and efficient HER photocatalytic systems in combination with transition-metal based NPs such as Ru NPs.^[14–16] However, even if the photocatalytic performance of the $\text{QuPh}^+\text{-NA}/\text{Ru}$ NPs system compares well with that of Pt-based systems under similar conditions, the organic dyad absorbs light mainly in the UV part of the electromagnetic spectrum and, due to its very low solubility in water, requires addition of organic solvents (i.e. MeCN) to the reaction media.

Herein we report our approach to attain efficient and durable visible-light-driven hydrogen evolution at neutral pH. This approach is based on the use of a ternary hybrid nanomaterial that combines TiO_2 -supported 4-phenylpyridine-capped Ru NPs as photocatalyst with an anchorable ruthenium trisbipyridine-based PA (RuP, Chart 1), and triethanolamine (TEOA) as SED. A detailed understanding of the electron transfer kinetics within the photochemical system examined is provided by time-resolved optical spectroscopy measurements, which evidence the key role of TiO_2 as electron-relay and highlight the electron transfer from the semiconductor to the Ru NPs as the rate-determining step prior to hydrogen evolution.

Results and discussion

Synthesis and characterization

The hybrid photocatalysts have been prepared in a three-step process (Scheme 1): 1) the organometallic approach for the synthesis of nanostructures, then 2) their deposition onto the TiO_2 surface by impregnation from a colloidal solution and finally 3) their controlled surface-oxidation. First, following our recent report,^[12] 4-phenylpyridine (PP) stabilized ruthenium NPs (RuPP) were synthesized by decomposing the $[\text{Ru}(\text{cod})(\text{cot})]$ (cod = 1,5-cyclooctadiene; cot = 1,3,5-cyclooctatriene) complex in THF under H_2 atmosphere (3 bar) at room temperature (r.t.), using PP as stabilizing ligand ($[\text{PP}]/[\text{Ru}] = 0.2$ molar equivalent). TEM analysis of the crude solution showed well-dispersed RuPP NPs of 1.4 ± 0.3 nm average diameter (by considering the smallest dimension) with a narrow size distribution (Figure 1a). Next, the crude colloidal RuPP solution was added to TiO_2 (at 2 and 10 wt.% Ru). The obtained slurry was stirred for 4 days at r.t. in the dark and under argon atmosphere. Then the solvent was filtered off which led to light/dark gray solids **RuPP(2%)- TiO_2** and **RuPP(10%)- TiO_2** , respectively, which were washed with hexane and dried under vacuum. Finally, the obtained nanomaterials were gradually exposed to air by slow oxygen diffusion at r.t. into a screw cap vial in which the solids were introduced under Ar, giving rise to the corresponding **Ru@RuO₂PP- TiO_2** nanohybrids (Scheme 1). This final protection step was performed in a controlled manner due to the known high reactivity of RuPP NPs when exposed to air, which alters their morphology and decreases their catalytic performance in

HER.^[12] The so-obtained hybrid nanomaterials were characterized by a set of complementary techniques.

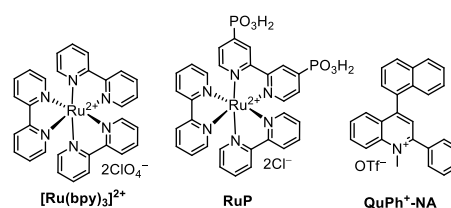
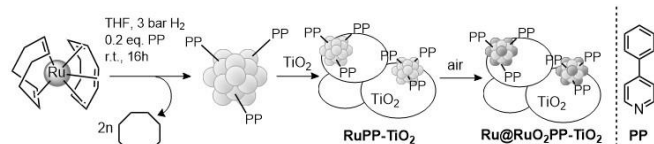


Chart 1. Molecular photoabsorbers used in this work.

Transmission electron microscopy (TEM) characterization of the **RuPP(2%)- TiO_2** and **RuPP(10%)- TiO_2** hybrids was carried out after depositing a drop of the slurry onto a carbon-covered copper grid. The deposition of small NPs onto the surface of TiO_2 crystals was observed for **RuPP(2%)- TiO_2** with no RuPP NPs visible outside of the grains (Figure S1a in the Supporting Information). Both isolated and supported NPs were observed for the **RuPP(10%)- TiO_2** sample (Figure S1b). Therefore, the study was continued only at low metal content, namely with **RuPP(2%)- TiO_2** sample. After a protection step by reacting with air, the **Ru@RuO₂PP- TiO_2** sample presented a Ru metal content of 1.6 wt.% as determined by ICP-OES analysis. Besides, HRTEM, HAADF-STEM (Figures 1b-d) and EDX (Figure S2) analyses on this sample evidenced the unaltered morphology and dispersion of the NPs in the hybrid materials after surface-oxidation. Fast Fourier Transform (FFT) electron diffraction patterns showed particles with crystalline character. Interplanar distances measured are indicative of the presence of both Ru and RuO_2 phases (Figure S3). The mean average diameter of the Ru/ RuO_2 NPs in the **Ru@RuO₂PP- TiO_2** sample calculated from HRTEM images (Figure 1b) is of 1.7 ± 0.4 nm. The chemical composition of the **Ru@RuO₂PP- TiO_2** sample was further analyzed by X-ray photoelectron spectroscopy (XPS). The mixture of metallic Ru and RuO_2 was confirmed (Figure S4), with Ru $3d_{5/2}$ peaks centered at 279.8 eV (metallic Ru) and 280.8 eV (RuO_2).

Photocatalytic hydrogen evolution

The photocatalytic performance of the nanomaterials towards the HER was evaluated in 0.2 M TEOA aqueous solution at pH 7 (25 °C) and, unless otherwise stated, under visible-light illumination ($\lambda > 400$ nm) calibrated to 1 sun intensity (see Figure S5 for a schematic representation of the employed setup). Together with TEOA as SED,^[17] the three molecular PAs shown in Chart 1 have been assayed in combination with **Ru@RuO₂PP** and **Ru@RuO₂PP- TiO_2** as HER (photo)catalysts. A summary of the obtained photocatalytic results can be found in Table 1.



Scheme 1. Synthesis of $\text{Ru@RuO}_2\text{PP-TiO}_2$.

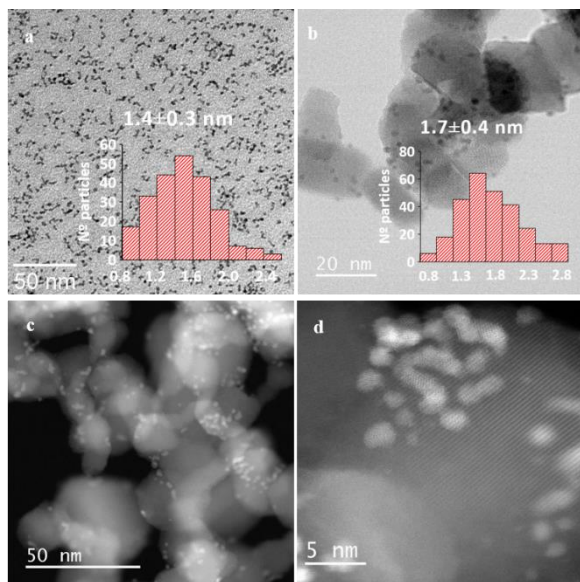


Figure 1. a) TEM image of RuPP nanoparticles and corresponding size histogram, b) TEM image of $\text{Ru@RuO}_2\text{PP-TiO}_2$ and corresponding size histogram, c) and d) HAADF-STEM images of $\text{Ru@RuO}_2\text{PP-TiO}_2$.

Initially, the photocatalytic performance of non-supported $\text{Ru@RuO}_2\text{PP}$ was assessed. The visible-light irradiation of a colloidal solution of $\text{Ru@RuO}_2\text{PP}$, TEOA and a PA among $[\text{Ru}(\text{bpy})_3]^{3+}$, RuP or QuPh⁺-NA showed no H₂ evolution (Figure 2a and Table 1, entries 1-3). The addition of methyl viologen (MV²⁺, entries 4-5) as an electron mediator did not lead to significant improvements, with H₂ evolution below 3.5 μmol after 10 h of irradiation. The low performance of the unsupported systems can be ascribed both to the low dispersibility and progressive aggregation of $\text{Ru@RuO}_2\text{PP}$ nanoparticles observed in aqueous media and to the inefficient charge accumulation within the nanoparticulate Ru catalysts leading to unfavorable charge recombination pathways.^[14] The latter hypothesis will be supported later on by photophysical data (see below). Finally, in contrast with the results of Fukuzumi and co-workers with the QuPh⁺-NA donor-acceptor dyad ($\lambda_{\text{max}} = 340 \text{ nm}$) combined with Ru NPs,^[14–16] when the $\text{Ru@RuO}_2\text{PP}$ / QuPh⁺-NA system was irradiated with the full solar spectrum (no UV filter applied in a quartz cell) no H₂ production was observed (Figure 2a and Table 1, entry 3). Thus, the results gathered with the unsupported $\text{Ru@RuO}_2\text{PP}$ nanomaterial highlight the need to improve the stability of this system in aqueous media and probably also the electronic communication/charge separation between it and visible-light

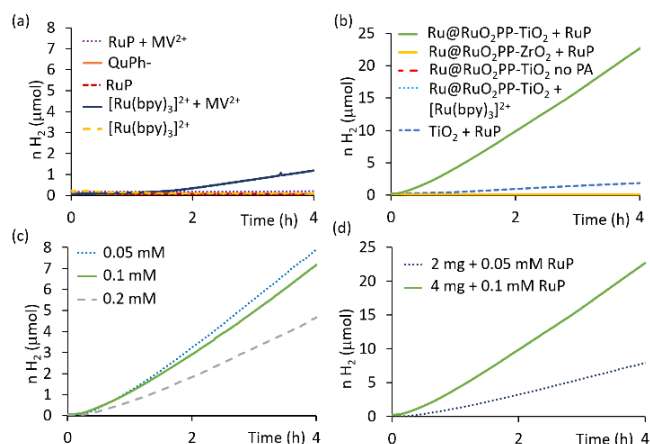


Figure 2. Photocatalytic hydrogen evolution in 4 mL of a 0.2 M TEOA aqueous solution of: (a) Unsupported $\text{Ru@RuO}_2\text{PP}$ with different PA (0.1 mM); (b) Supported $\text{Ru@RuO}_2\text{PP-MO}_2$ (M = Ti, Zr) with 0.1 mM $[\text{Ru}(\text{bpy})_3]^{2+}$, 0.1 mM RuP, no PA, and the corresponding TiO_2 -RuP blank; (c) Optimization of RuP PA concentration in the photocatalytic hydrogen evolution of $\text{Ru@RuO}_2\text{PP-TiO}_2$ (2 mg); (d) Study of the $\text{Ru@RuO}_2\text{PP-TiO}_2$ concentration at the optimized $\text{Ru@RuO}_2\text{PP-TiO}_2$ / RuP ratio.

PAs such as $[\text{Ru}(\text{bpy})_3]^{2+}$ or its derivatives. The effect of semiconducting TiO_2 as both NP support and/or electron-relay^[18–20] was then evaluated. The photocatalytic experiments with $\text{Ru@RuO}_2\text{PP-TiO}_2$ were performed in a pH neutral TEOA aqueous solution under visible light irradiation ($\lambda > 400 \text{ nm}$) and in the presence or absence of $[\text{Ru}(\text{bpy})_3]^{2+}$ and RuP as PAs (Table 1, entries 6-8). As shown in Figure 2b, hydrogen evolution was only observed in the presence of the RuP PA. The observed induction period may be ascribed to saturation of the aqueous solution prior to H₂ diffusion to the headspace (where the gas is measured), although the reduction of NP RuO_2 surface sites to more active metallic Ru under reductive conditions^[12] might also be considered. H₂ production also happened when bare TiO_2 was combined with RuP under visible light irradiation, even if at extremely slow reaction rates (Table 1, entry 10). These results emphasize the major role of both the TiO_2 support and the RuP PA phosphonic acid anchors in facilitating electron transfer and thus enabling HER photocatalysis. In contrast to non-supported $\text{Ru@RuO}_2\text{PP}$, the hybrid $\text{Ru@RuO}_2\text{PP-TiO}_2$ nanomaterial remains dispersed in the aqueous media and thus prevents deactivation by coalescence of the nanoparticulate catalyst under turnover conditions. As extensively reported, phosphonic acid groups are good TiO_2 anchors,^[21] although partial binding to the nanoparticle surface cannot be excluded. For a better understanding of the role of TiO_2 in the electron transfer between the Ru NPs and RuP in photocatalytic HER with $\text{Ru@RuO}_2\text{PP-TiO}_2$, TiO_2 was replaced by ZrO_2 in an analogous $\text{Ru@RuO}_2\text{PP-ZrO}_2$ hybrid that was prepared following the synthetic protocol described in Scheme 1 (see the Experimental Section and Figure S6 for further details on its synthesis and characterization). The mismatch between the potentials of the excited RuP and the ZrO_2 conduction band (CB) prevents the photoinduced charge separation between the dye and the metal oxide.¹⁸ As shown in Figure 2b and entry 9 in Table 1, no

H₂ evolution is observed when **Ru@RuO₂PP-ZrO₂**, RuP and TEOA are irradiated with visible-light in neutral water, which suggests no direct electron transfer between the PA and the catalyst and

thus confirms the electron-mediator role of TiO₂ in the **Ru@RuO₂PP-TiO₂** hybrid.

Table 1. Visible-light driven (1 sun, $\lambda > 400$ nm) H₂ evolution with **Ru@RuO₂PP**, **Ru@RuO₂PP-MO₂** (M = Ti or Zr, 4 mg) and **Ru@RuO₂PP-TiO₂-RuP** and different PA (when required, 0.1 mM) in 0.2 M TEOA buffer (4 mL) at pH 7 and 25 °C.

Entry	Material	Mass (mg)	$\mu\text{mol Ru}$	PA	$\mu\text{mol H}_2$ (10 h)	HE _{max} rate ($\mu\text{mol} \cdot \text{h}^{-1}$)	TOF _{max} ($\text{mol}_{\text{H}_2} \cdot \text{h}^{-1} \cdot \text{mol}_{\text{Ru}}^{-1}$)
1	Ru@RuO ₂ PP	0.04	0.35	[Ru(bpy) ₃] ²⁺	0	0	0
2	Ru@RuO ₂ PP	0.05	0.39	RuP	0	0	0
3	Ru@RuO ₂ PP	0.05	0.42	QuPh-NA ^{+(a)}	0	0	0
4	Ru@RuO ₂ PP	0.08	0.66	[Ru(bpy) ₃] ²⁺ + MV ^{2+(b)}	3.4	0.4	0.6
5	Ru@RuO ₂ PP	0.05	0.42	RuP + MV ^{2+(b)}	0.3	<0.01	<0.02
6	Ru@RuO ₂ PP-TiO ₂	4.00	0.63	[Ru(bpy) ₃] ²⁺	0	0	0
7	Ru@RuO ₂ PP-TiO ₂	4.00	0.63	RuP	58.2	6.4	10.2
8	Ru@RuO ₂ PP-TiO ₂	4.00	0.63	No PS	0	0	0
9	Ru@RuO ₂ PP-ZrO ₂	4.00	0.63	RuP	0	0	0
10	TiO ₂	4.00	-	RuP	3.3	0.5	-
11	Ru@RuO ₂ PP-TiO ₂ -RuP	4.00	0.63	-	110.7	12.6	21.5

[a] QuPh-NA⁺ solubilized in MeCN prior to injection in 4 mL TEOA buffer (6 mL quartz cell) under overall solar spectrum irradiation. [b] [MV²⁺] = 5 mM.

Once with an active photocatalytic system on hand, optimization of the RuP and **Ru@RuO₂PP-TiO₂** concentrations was carried out before proceeding to long-term stability analyses. First, three different RuP concentrations (0.05, 0.1 and 0.2 mM) were assayed under identical reaction conditions (Figure 2c). Maximum H₂ production rates were reached at low/medium RuP concentrations (0.05 and 0.1 mM). The unproductive absorption of light by non-anchored RuP molecules that remain in solution after TiO₂ surface saturation could be at the origin of the lower performance of the photocatalytic system at high concentrations of RuP (0.2 mM). UV-vis spectroscopy was employed to analyze the amount of bound/unbound RuP when mixed with 2 mg of the **Ru@RuO₂PP-TiO₂** hybrid. Thus, for both 0.05 and 0.1 mM solutions ca. 25% (0.0125 and 0.025 mM, respectively) of the added RuP was found to remain in solution against 36% (0.072 mM) for the 0.2 mM case (Figure S7). Accordingly, the increase of anchored RuP along the studied 0.05-0.2 mM range is not linear, being significantly reduced at high concentration (Figure S8). Thus, even if more RuP is anchored at the surface of **Ru@RuO₂PP-TiO₂** at 0.2 mM (513 nmol vs 300 nmol at 0.1 mM), the significant increase of unbound PA at this concentration (0.072 mM, Figure S7) decreases the performance of the photocatalytic system due to unproductive light absorption (compare entries 7 and 11 in Table 1). Finally, the variation of the quantity of **Ru@RuO₂PP-TiO₂** (2 and 4 mg) was studied at the optimum photocatalyst-RuP ratio showing a linear increase of the evolved hydrogen (Figure 2d).

In order to avoid the unproductive absorption of light resulting from unbound PA in solution, a **Ru@RuO₂PP-TiO₂-RuP** hybrid (where the RuP PA is previously bound to **Ru@RuO₂PP-TiO₂**) was prepared by mixing 4 mg of **Ru@RuO₂PP-TiO₂** and 0.1 mM RuP in 4 mL of water for 20 min followed by centrifugation (see Experimental Section and Figure S9 in the Supporting Information). The amount of RuP anchored in the resulting

yellowish solid was determined through both the absorption changes in the UV-vis spectra of the solution measured before and after the grafting process and ICP-OES/MS (1.6 wt.% Ru/0.07 wt.% P) analyses. As shown in Figure 3, when triggered by visible-light in 0.2 M TEOA aqueous solution the **Ru@RuO₂PP-TiO₂-RuP** hybrid shows superior HER performance than the **Ru@RuO₂PP-TiO₂** + RuP mixture, thus confirming the detrimental effect of unbound RuP in HER photocatalysis.

Under optimized conditions, visible-light ($\lambda > 400$ nm) irradiation at 1 sun intensity of **Ru@RuO₂PP-TiO₂-RuP** (4 mg) in 4 mL of 0.2 M TEOA aqueous solution yields 111 μmol of H₂ in 10 h and maximum H₂ evolution rate (HE_{max} rate) and turnover frequency (TOF_{max}) of 12.6 $\mu\text{mol} \cdot \text{h}^{-1}$ and 21.5 $\text{mol}_{\text{H}_2} \cdot \text{h}^{-1} \cdot \text{mol}_{\text{Ru}}^{-1}$, respectively (Table 1, entry 11). An apparent quantum yield (AQY) of 1.3 % has been determined under these optimized conditions (see ESI for the detailed calculation). The long-term stability of the photocatalytic system was evaluated under the same optimized conditions, evolving 280 μmol of H₂ after 130 h under visible-light irradiation (Figure 3a). This durability is remarkable, particularly when compared to photochemical systems involving TiO₂-supported molecular catalysts^{18,28} (see Table S1 for details), in which fast deactivation due to catalyst degradation typically occurs under operative conditions. Comparing the HER performance of different photocatalyst is not an easy task given the lack of a common benchmarking protocol and the various conditions in which they are tested. However, the main photocatalytic data of **Ru@RuO₂PP-TiO₂-RuP** and those of literature examples based on TiO₂-supported Ru- or Pt-based nanocatalysts are shown in Table S1 together with TiO₂-supported systems involving molecular catalysts. In this respect, our **Ru@RuO₂PP-TiO₂-RuP** hybrid displays comparable performances with respect to Pt-based supported systems in terms of amount of hydrogen produced albeit with slower rates, whereas clearly outperforms TiO₂-supported molecular catalysts particularly as far as long-term stability is

concerned. For further comparison, in Table S2 are collected the photocatalytic data obtained on unsupported Ru- and Pt-based systems which, as previously suggested, definitely prove the relevance of the TiO₂ support in enabling photoinduced hydrogen evolution by the **Ru@RuO₂PP** catalyst.

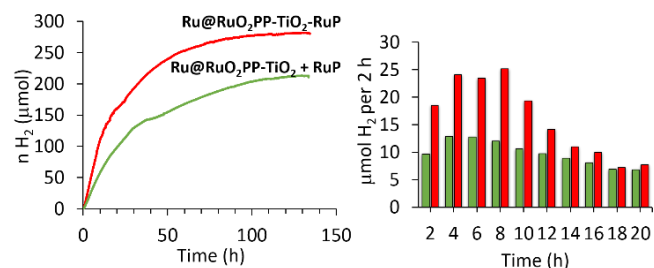


Figure 3. Photocatalytic hydrogen evolution profile (left) and hydrogen evolution rate per 2 h (right) for **Ru@RuO₂PP-TiO₂** (4 mg) + [RuP] = 0.1 mM (green) and **Ru@RuO₂PP-TiO₂-RuP** (red) under visible-light irradiation in a 4 mL TEOA 0.2 M aqueous solution at pH 7.

Under optimized conditions, a progressive decrease of the H₂ evolution rate with time is observed along the time course of photocatalysis (i.e. HE_{max} = 12.6 μmol · h⁻¹ vs. HE_{18h-20h} = 7.5 μmol · h⁻¹, see Figure 3b). Considering the maximum amount of hydrogen produced (280 μmol), the initial amount of TEOA present in solution (800 μmol), as well as the two-electron nature of the latter as a SED,^[17] we can estimate that only 35% TEOA is consumed after 130 h of irradiation, thus suggesting that consumption of the SED can be ruled out as a possible reason for photocatalysis deactivation.

Hence, with the aim of understanding the origin of the observed decrease and eventual cessation of photocatalytic activity, the fate of the **Ru@RuO₂PP-TiO₂** photocatalyst after the long photocatalytic run was studied by both TEM (Figure S10) and ICP-OES/MS analyses. A carbon covered copper grid was prepared by depositing a drop of the slurry at the end of the photocatalytic experiment. The TEM image (Figure S10) shows both (1) the presence of isolated NPs leached from the TiO₂ surface and, (2) agglomeration of the hybrid nanomaterial under turnover conditions. Thus, the mechanical instability of the RuPPNPs-TiO₂ interface and the aggregation of the hybrid nanomaterial can be at the origin of the observed decrease in photocatalytic activity.

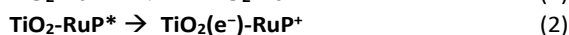
Additionally, the **Ru@RuO₂PP-TiO₂-RuP** photocatalyst was recovered from the photocatalytic cell by centrifugation followed by washing with water, isopropanol and diethyl ether and drying under vacuum. ICP-OES/MS analyses of the resulting brown solid indicated Ru and P contents of 0.4 wt.% and 0.07 wt.%, respectively. From the P content the amount of RuP anchored to the photocatalyst surface could be estimated and, therefore, the wt.% Ru arising from **Ru@RuO₂PP** NPs that remains in the sample after photocatalysis, namely 0.29 wt.%. Considering the wt.% of Ru and P present in the as-synthesized **Ru@RuO₂PP-TiO₂-RuP** hybrid (1.6 wt.% and 0.07 wt.%, respectively), this value indicates that 82 % of the Ru content

have leached from the TiO₂ surface after 130 h of photocatalysis.

Photophysical Analysis

The kinetic analysis of the electron transfer events occurring upon irradiation was performed by a combination of time-resolved emission and absorption spectroscopic studies on thin films immersed in aqueous solutions under N₂-purged conditions (see Experimental Section for further details).

The primary photochemical process was established by means of time-resolved luminescence analysis upon 532-nm excitation by recording the emission intensity at 620 nm (Figure 4). As is apparent, negligible emission is observed when the RuP chromophore is attached onto TiO₂ (**TiO₂-RuP**) when compared to the result obtained for the same dye onto ZrO₂ (**ZrO₂-RuP**). This is in agreement with the expected quenching of the RuP excited state by electron injection into the TiO₂ conduction band (E_{CB} = -0.7 V vs. NHE at pH 7),^[18] unfeasible in the case of ZrO₂ (E_{CB} = -1.4 V vs. NHE at pH 7).^[22] This process is indeed expected to occur with almost unitary efficiency within <100 ps.^[23] Interestingly, negligible quenching of the luminescence is observed with RuP onto ZrO₂ in the presence of either the catalyst (**Ru@RuO₂PP-ZrO₂-RuP**) or the TEOA sacrificial donor (**ZrO₂-RuP/TEOA**) where the lifetime of the RuP excited state appreciably matches the one of RuP alone (**ZrO₂-RuP**, τ ~ 330 ns, see Figure S11 for related fittings). These results thus confirm that in the **Ru@RuO₂PP-TiO₂-RuP/TEOA** system the primary photochemical event is the ultrafast electron injection from the excited state of the RuP chromophore to the TiO₂ conduction band leading to an oxidized RuP⁺ species at the surface and a formally reduced semiconductor (eqs 1,2).



Furthermore, the failure to observe any quenching of the RuP excited state in both **Ru@RuO₂PP-ZrO₂-RuP** and **ZrO₂-RuP/TEOA** suggests the inefficiency of both oxidative quenching by the **Ru@RuO₂PP** catalyst and reductive quenching by TEOA. This result supports the observation of negligible hydrogen evolution activity in the absence of TiO₂ (see Table 1) and points towards the fundamental requirement of the semiconductor as an electron-transfer mediator for efficient hydrogen production.

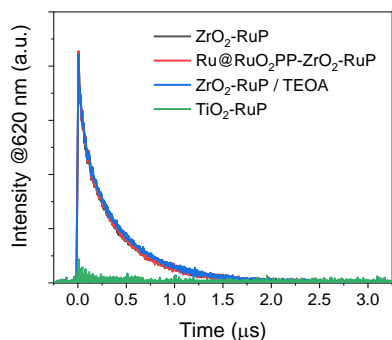


Figure 4. Time-resolved luminescence decays measured at 620 nm by laser flash photolysis (excitation at 532 nm) of thin films in N_2 -purged aqueous solutions: **ZrO₂-RuP** in 0.1 M Na_2SO_4 at pH 7 (black trace), **Ru@RuO₂PP-ZrO₂-RuP** in 0.1 M Na_2SO_4 at pH 7 (red trace), **ZrO₂-RuP** in 0.2 M TEOA at pH 7 (blue trace), and **TiO₂-RuP** in 0.1 M Na_2SO_4 at pH 7 (green trace).

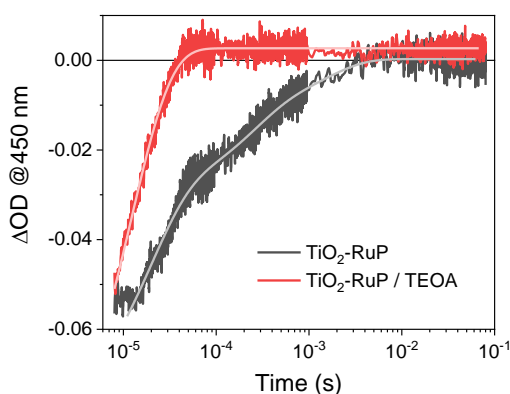


Figure 5. Transient absorption kinetics at 450 nm measured by laser flash photolysis (excitation at 532 nm) of **TiO₂-RuP** in N_2 -purged aqueous solutions containing 0.1 M Na_2SO_4 at pH 7 (black trace) and 0.2 M TEOA at pH 7 (red trace).

The subsequent electron transfer events were then monitored by transient absorption spectroscopy. The electron transfer from the TEOA sacrificial donor to the oxidized RuP chromophore was followed upon 532-nm excitation of **TiO₂-RuP** by looking at the decay of the transient signal at 450 nm corresponding to the bleaching of the metal-to-ligand charge transfer (MLCT) transition characteristic of the RuP^+ species (Figure 5).^[24] In the absence of the electron donor this transient signal decays to the baseline with a complex kinetics which requires three-exponentials for a reasonable fitting.^[25] An average lifetime of $\tau = 0.37$ ms can be estimated (Figure S12). This process can be assigned to the charge recombination between the oxidized RuP chromophore and the electron in the TiO_2 conduction band (eq 3). The complex kinetics observed is indeed characteristic of such a recombination process.^[25,26]



In the presence of the TEOA donor (0.2 M, pH 7) the transient signal at 450 nm decays more rapidly and this is attributable to a fast recovery of the RuP ground-state via electron transfer from the TEOA to the RuP^+ species (eq 4). The oxidized TEOA is then expected to decompose upon electron transfer (eq 5).^[17] A lifetime of $\tau = 12.1$ μs can be estimated for RuP^+ in the presence of 0.2 M TEOA at pH 7 from a single-exponential fitting of the kinetic trace (Figure S12). This value translates into ca. 97% efficiency for the hole scavenging process from the photogenerated oxidized chromophore under the experimental conditions used in the hydrogen evolution experiments. Overall, these data are consistent with those reported on a similar photochemical system.^[18]

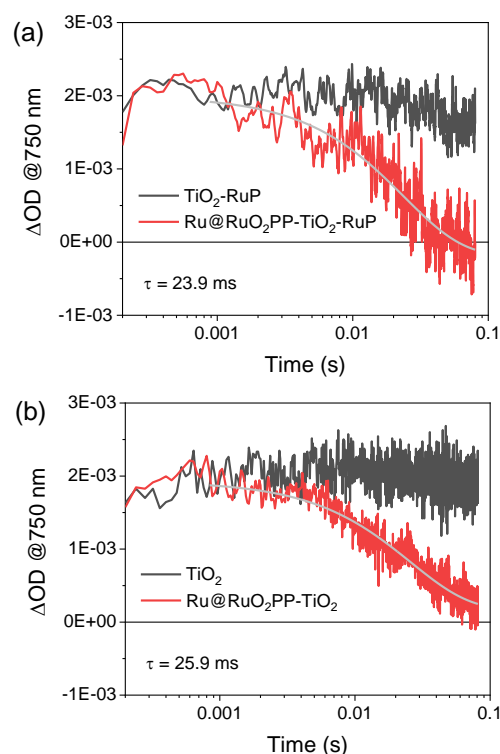
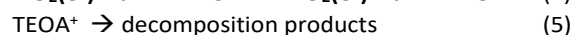


Figure 6. Transient absorption kinetics at 750 nm measured by laser flash photolysis of thin films in N_2 -purged aqueous solutions containing 0.2 M TEOA at pH 7: (a) excitation at 532 nm of **Ru@RuO₂PP-TiO₂-RuP** and **TiO₂-RuP**, (b) excitation at 355 nm of **Ru@RuO₂PP-TiO₂** and **TiO₂**.

Due to the irreversible nature of the TEOA oxidation process (eq 5), RuP^+ reduction by the sacrificial donor leads to accumulation of electrons in the TiO_2 conduction band (eq 4,5). The fate of these electrons was followed by transient absorption spectroscopy from the featuring absorption in the red portion of the visible spectrum.²⁷ Dye excitation at 532 nm in **TiO₂-RuP** in the presence of TEOA produces a permanent transient

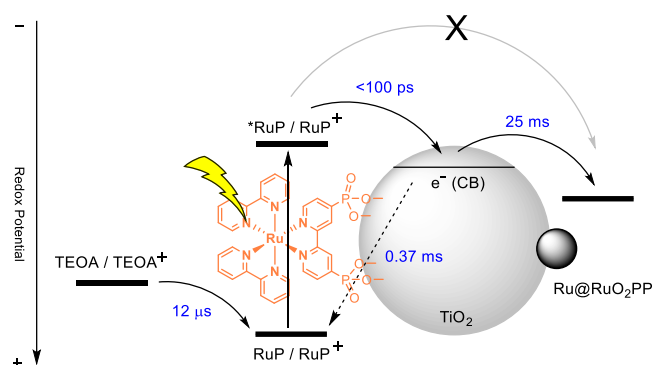
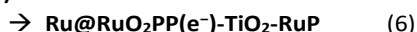


Figure 7. Schematic representation of the processes and kinetics of the electron transfer events occurring upon irradiation of the **Ru@RuO₂PP-TiO₂-RuP/TEOA** system.

absorption at 750 nm attributable to long-lived electrons in the TiO₂ conduction band. This transient signal remains indeed constant within the time-window of the experiment (Figure 6a, black trace). The same transient absorption is still present upon 532-nm excitation of the **Ru@RuO₂PP-TiO₂-RuP** system in 0.2 M TEOA. However, this is observed to decay to the baseline within ca. 100 ms (Figure 6a, red trace). This evidence can be attributed to the reduction of the **Ru@RuO₂PP** catalyst by electrons in the TiO₂ conduction band (eq 6).

Ru@RuO₂PP -TiO₂(e⁻)-RuP



Interestingly, comparable results are obtained in the absence of the RuP chromophore upon band-gap excitation at 355 nm of the TiO₂ semiconductor in the **Ru@RuO₂PP-TiO₂** photocatalyst (Figure 6b), thus confirming the mechanistic assignment. A time-constant of $\tau = 25$ ms can be estimated for the electron transfer from the TiO₂ conduction band to the **Ru@RuO₂PP** nanoparticles. This value is considerably larger than the one observed for the electron transfer from TiO₂ to two different molecular catalysts, namely a cobaloxime and a nickel(II) bis(diphosphine) complex,^[18,28] apparently suggesting a greater inertness of the nanoparticulate material towards electron transfer with respect to molecular species.‡ Furthermore, under continuous irradiation and concomitant electron accumulation within the catalytic **Ru@RuO₂PP** unit the Fermi level of the ruthenium nanoparticle is expected to up-shift.²⁹ Accordingly, before hydrogen elimination, electron transfer from the TiO₂ conduction band to **Ru@RuO₂PP** is expected to become progressively less favorable on thermodynamic grounds and, as a consequence, kinetically slower. Taken together, considering the sequence of photo-triggered electron transfer processes previously discussed, these results unavoidably point towards the identification of the electron accumulation within the catalytic **Ru@RuO₂PP** as the rate-determining step in light-driven hydrogen evolution by the **Ru@RuO₂PP-TiO₂-RuP/TEOA** system. The whole series of electron transfer events is summarized in Figure 7.

Experimental

Materials and methods

4-phenylpyridine ligand and titanium dioxide P-25 anatase/rutile (TiO₂) were purchased from *Sigma Aldrich* and dried through vacuum/Ar cycles before their use. 0.2 M MilliQ aqueous solution of triethanolamine (*Sigma Aldrich*) was adjusted to pH 7 by the addition of HCl. The organometallic precursor [Ru(cod)(cot)] was commercially obtained from *Nanomeps*. All solvents (Scharlab) were distilled over Na/benzophenone (THF) or CaH₂ (hexane) and degassed by freeze-pump-thaw cycles. H₂ and Ar were purchased from *Alphagaz*. The synthesis of the nanoparticles was performed under Ar inert atmosphere using Schlenk line techniques or a glovebox (MBraun Unilab Worskstation 9550). The photosensitizers [Ru(bpy)₃](ClO₄)₂ and [Ru(bpy)₂(4,4'-(PO₃H₂)₂(bpy))]Cl₂ (RuP) were synthesized from procedures previously described in the literature.^[30–32] 2-Phenyl-4-(1-naphthyl)quinolinium triflate (QuPh⁺-NA) was synthesized following a reported method.^[33]

Synthesis of supported Ru NPs onto TiO₂ (Ru@RuO₂PP-TiO₂). 4-phenylpyridine-capped Ru nanoparticles (RuPP NPs) were prepared following a previous report¹² by exposing under hydrogen atmosphere (3 bar) a mixture of 150 mg (0.476 mmol) of [Ru(cod)(cot)] and 15 mg (0.095 mmol) of 4-phenylpyridine (PP) in dried and degassed THF in a Fischer Porter bottle for 16 h. One drop of the resulting colloidal solution was deposited onto a carbon covered copper grid for TEM characterization (mean diameter = 1.4 ± 0.3 nm). 12.8 mL or 64 mL of the colloidal black solution was then added under Ar onto 200 mg of TiO₂ placed in two independent Schlenk flasks and the mixtures were stirred for 4 days in the dark. The solvent was filtered off and the materials were washed with hexane (10 mL, 3 times) by cannula to obtain RuPP(2%)-TiO₂ or RuPP(10%)-TiO₂ as grey solids. The obtained RuPP(2%)-TiO₂ nanomaterial was placed into an Ar-filled screw cap vial and gradually exposed to air by slow oxygen diffusion at r.t. (20 days), yielding the corresponding **Ru@RuO₂PP-TiO₂** nanohybrid. ICP-OES characterization of **Ru@RuO₂PP-TiO₂** indicated a ruthenium content of 1.6 Ru wt.%.

Synthesis of supported RuPP NPs onto ZrO₂ (Ru@RuO₂PP-ZrO₂). Following the same procedure described above for the preparation of **Ru@RuO₂PP-TiO₂**, the addition of 2.55 mL of the RuPP colloidal solution onto 40 mg of ZrO₂ yields **Ru@RuO₂PP-ZrO₂** after slow surface-oxidation. ICP-OES: 1.6 Ru wt.%.

Synthesis of Ru@RuO₂PP-TiO₂-RuP. 4 mg of **Ru@RuO₂PP-TiO₂** and 4 mL of (MilliQ) water were added to a vial containing a stir bar. The solid was sonicated for 5 min until total dispersion of the material. Then, 80 μL of an aqueous solution of RuP (5 mM) were added to the dispersion and the resulting suspension was stirred for 15 min. The solid was isolated by centrifugation (10 min, 2000 rpm) and washed 3 times with water. ICP characterization of **Ru@RuO₂PP-TiO₂-RuP** indicated a

ruthenium content of 1.6 wt.% (ICP-OES) and phosphorus content of 0.07 wt.% (ICP-MS).

Characterization

Transmission Electron Microscopy (TEM), High-Resolution Electron Microscopy (HRTEM), Energy-dispersive X-ray spectroscopy (EDX), High-Angle Annular Dark-Field Scanning Transmission Electron Microscopy (HAADF-STEM) and electron diffraction analysis were performed either in a JEOL 1400 microscope operating at 100kV at the “Servei de Microscopia Electronica” of the UAB or in a JEOL JEM 1011 microscope operating at 100kV with a resolution point of 0.45 nm or in a JEOL JEM-ARM 200F microscope working at 200kV with a resolution point lower of 0.19 nm at the “Centre de Microcaracterisation Raymond Castaing” in UMS-CNRS 3623. Samples were prepared by deposition of some drops of dispersed material in a solvent onto a carbon covered copper grid. Micrographs were treated with ImageJ to obtain the statistical size distribution of the nanoparticles, assuming that they were spherical. NP sizes are quoted as the mean diameter \pm the standard deviation. Inductive-Coupled Plasma (ICP-OES and ICP-MS) measurements were performed at the “Servei d'Anàlisi Quimica” (SAQ) in the UAB, on an Optima 4300DV Perkin-Elmer system. Solid samples were prepared by digesting 1 mg of the RuPPNPs-TiO₂ with *aqua regia* under microwave conditions followed by a dilution of the mixture with HCl 1 % (v/v). The samples were microfiltered (0.45 μ m) prior to injection to eliminate white colloidal TiO₂. X-ray Photoelectron Spectroscopy (XPS) measurements were performed at the Catalan Institute of Nanoscience and Nanotechnology (ICN2) in Barcelona with a Phoibos 150 analyzer (SPECS GmbH, Berlin, Germany) in ultra-high vacuum conditions (base pressure 5×10^{-10} mbar) with a monochromatic aluminium K α X-ray 456 source (1486.74 eV). The energy resolution was measured by the FWHM of the Ag 3d_{5/2} peak which for a sputtered silver foil was 0.62 eV.

Photocatalytic experiments

Hydrogen evolved was measured by using a Clark hydrogen electrode (Unisense H2-NP-9463). The photocatalytic hydrogen evolution reaction was performed in a 6 mL glass cell thermostated at 25 °C, containing 4 mL of 0.2 M TEOA as SED in which the photocatalyst was dispersed in the dark in an ultrasounds bath for 5 min. The cell was sealed with a septum and grease and the Clark electrode tip was introduced at the headspace of the cell (Figure S5). The solution was degassed with Ar bubbling for at least 10 min until stabilization of the signal. A concentrated water solution of the photosensitizer was injected. A flat signal was recorded for at least 2 min. Then, the cell was irradiated with a solar simulator (Abet 10500) containing a Xe lamp placed at exactly 1 sun (100 mW/cm²) distance. After recording the hydrogen evolution, the cell was degassed by Ar bubbling and a calibration was performed by injecting known volumes of H₂ (usually 50, 100, 150, 200, 250, 300 and 400 μ L, Figure S13) with a Hamilton syringe for gases.

Photophysical experiments

Time-resolved emission and absorption measurements were performed with a custom laser spectrometer comprised of a Continuum Surelite II Nd:YAG laser (FWHM 6 – 8 ns) with frequency doubled (532 nm) or tripled (355 nm) option, an Applied Photophysics xenon light source including a mod. 720 150W lamp housing, a mod. 620 power-controlled lamp supply and a mod. 03 –102 arc lamp pulser. Laser excitation was provided at 90° with respect to the white light probe beam. Light emitted or transmitted by the sample was focused onto the entrance slit of a 300 mm focal length Acton SpectraPro 2300i triple grating, flat field, and double exit monochromator equipped with a photomultiplier detector (Hamamatsu R3896). Signals from the photomultiplier were processed by means of a TeledyneLeCroy 604Zi (400 MHz, 20 GS/s) digital oscilloscope. The excitation pulse (either of 532 or 355 nm wavelength) was defocused using a diverging lens and set to an average energy of \sim 5 mJ/pulse using a combination of neutral density filters (Edmund Optics). Measurements were carried out at pH 7 in the presence of either 0.2 M TEOA or 0.1 M Na₂SO₄, the solutions were purged with nitrogen for 20 minutes before each experiment. TiO₂ and ZrO₂ thin films were prepared by doctor-blading of TiO₂ or ZrO₂ paste onto FTO-covered glasses (20 cm \times 20 cm, TEC 8, 8 Ω /cm, purchased from Pilkington) followed by calcination at 500 °C for 30 min. An active surface area of 1.5 cm² was achieved. The TiO₂ paste was commercial (18NR-T, GreatCell-Solar), while the ZrO₂ paste was prepared according to the literature.³⁴ Adsorption of RuP onto TiO₂ or ZrO₂ thin films was performed by soaking overnight the electrode into a 0.1 mM RuP solution in ethanol providing an absorbance of \sim 0.6 at the maximum of the MLCT transition. Deposition of **Ru@RuO₂PP** was performed by dispersion of the nanomaterial in a THF solution (concentration approximately 2-3 mg/mL) followed by spin-coating (3 steps, each of 20 seconds at 2000 rpm). In the three-component sample (**Ru@RuO₂PP-TiO₂-RuP**) deposition of **Ru@RuO₂PP** was made prior to soaking into the RuP solution.

Conclusions

Summarizing, a ternary hybrid nanomaterial, **Ru@RuO₂PP-TiO₂-RuP**, has been prepared through a synthetic protocol comprising the organometallic synthesis of ruthenium nanoparticles stabilized by the 4-phenylpyridine ligand (RuPP), the deposition of the RuPP NPs onto TiO₂ by impregnation of the support, and the sensitization of the latter with a visible-light photoabsorber bearing phosphonic acid anchors (RuP). When combined with TEOA as SED, the **Ru@RuO₂PP-TiO₂-RuP** nanomaterial is able to promote efficient visible-light-driven HER photocatalysis for more than 100 h, yielding TON and TOF values over 480 mol_{H₂} \cdot mol_{Ru}⁻¹ and 21.5 mol_{H₂} \cdot h⁻¹ \cdot mol_{Ru}⁻¹, respectively, with an AQY of 1.3%. Photophysical investigation by means of time-resolved spectroscopic techniques provided a proper description of the photoinduced dynamics within the hybrid photocatalytic system and pointed towards the identification of the electron accumulation within the

Ru@RuO₂PP catalyst as the rate-limiting step in the photocatalysis. The combined photocatalytic and photophysical analysis allowed identifying the double key role of TiO₂ in this HER photocatalytic system. First, TiO₂ acts as an efficient dispersing agent for the nanoparticulate catalyst (**Ru@RuO₂PP**) under aqueous conditions, thus preventing its fast coagulation and consequent reduction of the accessible active sites. Second, it enables the electronic communication between the catalyst (**Ru@RuO₂PP**) and the anchored molecular photoabsorber (RuP) under visible-light irradiation, acting as a competent (and necessary) electron-relay. Thus, the double role of TiO₂ as both support and electron-mediator allows to attain, to our knowledge for the first time, efficient visible-light-driven HER photocatalysis combining a Ru-based photocatalyst and a molecular photoabsorber.

Conflicts of interest

There are no conflicts to declare.

Acknowledgements

This work was financially supported by the MINECO/FEDER project CTQ2015-64261-R, the CNRS and the University Paul Sabatier – Toulouse. M.N. acknowledges the University of Ferrara (FAR2019) for funding. RBG acknowledges Conselho Nacional de Desenvolvimento Científico e Tecnológico for the studentship (No. 142440/2015-9), to Fundo de Apoio ao Ensino, à Pesquisa e à Extensão – Universidade Estadual de Campinas (FAEPEX-UNICAMP), and to Prof. Dr. André Luiz Barboza Formiga. J.G.-A. acknowledges Serra Hünter Program. The authors acknowledge Guillaume Sauthier for XPS analysis.

Notes and references

‡ The observation of comparable quantum yields for hydrogen evolution in this work and in ref. 18 (involving a cobaloxime catalyst supported on TiO₂) strongly suggests that beside the first ET step from the TiO₂ CB to the catalyst, the subsequent ET events have also a strong impact on the overall hydrogen evolution rate. In this respect, the second ET from the TiO₂ CB to a reduced cobaloxime catalyst (involving Co(II)→Co(I) reduction) is indeed expected to be 10⁵ times slower than the first ET event (involving Co(III)→Co(II) reduction).³⁵

- N. S. Lewis, *Science*, 2016, **351**, aad1920–aad1920.
- A. González-Garay, M. S. Frei, A. Al-Qahtani, C. Mondelli, G. Guillén-Gosálbez and J. Pérez-Ramírez, *Energy Environ. Sci.*, 2019, **12**, 3425–3436.
- J. R. McKone, N. S. Lewis and H. B. Gray, *Chem. Mater.*, 2014, **26**, 407–414.
- K. Takijiri, K. Morita, T. Nakazono, K. Sakai and H. Ozawa, *Chem. Commun.*, 2017, **53**, 3042–3045.
- M. Li, K. Duanmu, C. Wan, T. Cheng, L. Zhang, S. Dai, W. Chen, Z. Zhao, P. Li, H. Fei, Y. Zhu, R. Yu, J. Luo, K. Zang, Z. Lin, M. Ding, J. Huang, H. Sun, J. Guo, X. Pan, W. A. Goddard, P. Sautet, Y. Huang and X. Duan, *Nat. Catal.*, 2019, **2**, 495–503.
- C. C. L. McCrory, S. Jung, I. M. Ferrer, S. M. Chatman, J. C. Peters and T. F. Jaramillo, *J. Am. Chem. Soc.*, 2015, **137**, 4347–4357.
- J. Creus, J. De Tovar, N. Romero, J. García-Antón, K. Philippot, R. Bofill and X. Sala, *ChemSusChem*, 2019, **12**, 2493–2514.
- J. Yu, Q. He, G. Yang, W. Zhou, Z. Shao and M. Ni, *ACS Catal.*, 2019, **9**, 9973–10011.
- S. Han, Q. Yun, S. Tu, L. Zhu, W. Cao and Q. Lu, *J. Mater. Chem. A*, 2019, **7**, 24691–24714.
- C. Amiens, D. Ciuculescu-Pradines and K. Philippot, *Coord. Chem. Rev.*, 2016, **308**, 409–432.
- R. Matheu, I. A. Moreno-Hernandez, X. Sala, H. B. Gray, B. S. Brunschwig, A. Llobet and N. S. Lewis, *J. Am. Chem. Soc.*, 2017, **139**, 11345–11348.
- J. Creus, S. Drouet, S. Suriñach, P. Lecante, V. Collière, R. Poteau, K. Philippot, J. García-Antón and X. Sala, *ACS Catal.*, 2018, **8**, 11094–11102.
- Y. Yamada, S. Shikano and S. Fukuzumi, *J. Phys. Chem. C*, 2013, **117**, 13143–13152.
- S. Fukuzumi and Y. Yamada, *J. Mater. Chem.*, 2012, **22**, 24284–24296.
- Y. Yamada, T. Miyahigashi, H. Kotani, K. Ohkubo and S. Fukuzumi, *J. Am. Chem. Soc.*, 2011, **133**, 16136–16145.
- Y. Yamada, T. Miyahigashi, K. Ohkubo and S. Fukuzumi, *Phys. Chem. Chem. Phys.*, 2012, **14**, 10564–10571.
- Y. Pellegrin and F. Odobel, *Comptes Rendus Chim.*, 2017, **20**, 283–295.
- F. Lakadamyali, A. Reynal, M. Kato, J. R. Durrant and E. Reisner, *Chem. - A Eur. J.*, 2012, **18**, 15464–15475.
- M. A. Melo, Z. Wu, B. A. Nail, A. T. De Denko, A. F. Nogueira and F. E. Osterloh, *Nano Lett.*, 2018, **18**, 805–810.
- W. Kim, E. Edri and H. Frei, *Acc. Chem. Res.*, 2016, **49**, 1634–1645.
- E. B. And and W. Choi, *J. Phys. Chem. B*, 2006, **110**, 14792–14799.
- K. Hara, K. Miyamoto, Y. Abe and M. Yanagida, *J. Phys. Chem. B*, 2005, **109**, 23776–23778.
- D. F. Zigler, Z. A. Morseth, L. Wang, D. L. Ashford, M. K. Brennaman, E. M. Grumstrup, E. C. Brigham, M. K. Gish, R. J. Dillon, L. Alibabaei, G. J. Meyer, T. J. Meyer and J. M. Papanikolas, *J. Am. Chem. Soc.*, 2016, **138**, 4426–4438.
- M. Natali, M. Orlandi, S. Berardi, S. Campagna, M. Bonchio, A. Sartorel and F. Scandola, *Inorg. Chem.*, 2012, **51**, 7324–7331.
- R. R. Knauf, M. K. Brennaman, L. Alibabaei, M. R. Norris and J. L. Dempsey, *J. Phys. Chem. C*, 2013, **117**, 25259–25268.
- T. A. Heimer, E. J. Heilweil, C. A. Bignozzi and G. J. Meyer, *J. Phys. Chem. A*, 2000, **104**, 4256–4262.
- A. Kafizas, X. Wang, S. R. Pendlebury, P. Barnes, M. Ling, C. Sotelo-Vazquez, R. Quesada-Cabrera, C. Li, I. P. Parkin and J. R. Durrant, *J. Phys. Chem. A*, 2016, **120**, 715–723.
- M. A. Gross, A. Reynal, J. R. Durrant and E. Reisner, *J. Am. Chem. Soc.*, 2014, **136**, 356–366.
- W. Bi, L. Zhang, Z. Sun, X. Li, T. Jin, X. Wu, Q. Zhang, Y. Luo, C. Wu and Y. Xie, *ACS Catal.*, 2016, **6**, 4253–4257.
- M. R. Norris, J. J. Concepcion, C. R. K. Glasson, Z. Fang, A.

- M. Lapidés, D. L. Ashford, J. L. Templeton and T. J. Meyer, *Inorg. Chem.*, 2013, **52**, 12492–12501.
- 31 D. L. Ashford, M. K. Brennaman, R. J. Brown, S. Keinan, J. J. Concepcion, J. M. Papanikolas, J. L. Templeton and T. J. Meyer, *Inorg. Chem.*, 2015, **54**, 460–469.
- 32 P. Jansa, O. Baszczyński, E. Procházková, M. Dračinský and Z. Janeba, *Green Chem.*, 2012, **14**, 2282–2288.
- 33 H. Kotani, K. Ohkubo and S. Fukuzumi, *Faraday Discuss.*, 2012, **155**, 89–102.
- 34 A. Orbelli Biroli, F. Tessore, M. Pizzotti, C. Biaggi, R. Ugo, S. Caramori, A. Aliprandi, C. A. Bignozzi, F. De Angelis, G. Giorgi, E. Licandro and E. Longhi, *J. Phys. Chem. C*, 2011, **115**, 23170–23182.
- 35 A. Reynal, F. Lakadamyali, M. A. Gross, E. Reisner and J. R. Durrant, *Energy Environ. Sci.*, 2013, **6**, 3291–3300.